ARTICLE

Two-Dimensional VDW Crystal SnP_3 with High Carrier Mobility and Extraordinary Sunlight Absorbance

Chen Wang, Ting Hu*, Erjun Kan*

Department of Applied Physics and Institution of Energy and Microstructure, Nanjing University of Science and Technology, Nanjing 210094, China

(Dated: Received on September 21, 2018; Accepted on October 17, 2018)

Although bulk SnP_3 has been fabricated by experiments in the 1970's, its electronic and optical properties within several layers have not been reported. Here, based on first-principles calculations, we have predicted two-dimensional SnP_3 layers as new semiconducting materials that possess indirect band gaps of 0.71 eV (monolayer) and 1.03 eV (bilayer), which are different from the metallic character of bulk structure. Remarkably, 2D SnP_3 possesses high hole mobility of 9.171×10^4 $cm^2\cdot V^{-1}\cdot s^{-1}$ and high light absorption ($\sim10^6$ cm^{-1}) in the whole visible spectrum, which predicts 2D SnP_3 layers as prospective candidates for nanoelectronics and photovoltaics. Interestingly, we found that 2D SnP_3 bilayer shows similar electronic and optical characters of silicon.

Key words: Stannum phosphide, Electronic properties, First-principles calculations, Semiconductor

I. INTRODUCTION

Since the successful isolation of graphene by mechanical exfoliation in 2004 [1–5], two-dimensional (2D) materials have become a hot topic in the research of basic science and advanced technology owing to their rich phenomena, exceptional properties, and promising applications in nanoscale devices [6–16]. However, the absence of band gap of graphene has limited its applications in real electric devices. Consequently, 2D materials with moderate band gap, suitable optical gap, and high carriers mobility become more and more important. Previously, atomically thin MoS_2 monolayer with a direct band gap of 1.8 eV has been endowed great potential in electronics and photonics applications [17–20], however, the rich intrinsic defects severely reduce the carriers mobility [21, 22]. For phosphorene, it has been long-standing challenge to maintain its desired gap and high hole mobility [23–28]. On the other hand, hexagonal boron nitride monolayer is not an ideal candidate for optoelectronic or electric devices due to its wide band gap [29–31]. Therefore, 2D crystals with moderate band gaps and optical properties are still highly sought for efficient photovoltaic and optoelectronic applications [32].

Recently, some new 2D semiconductors have been predicted with suitable band gaps [33–36]. Considering the great development of today's technology and optoelectronics based on silicon, searching new 2D semiconductors with similar properties of silicon may provide various candidates for the applications. Here, in this work, we demonstrated a new semiconductor, *i.e.*, 2D SnP_3 bilayer, which has the similar electronic and optical properties of silicon. As a layered compound of Sn-P system, tin triphosphide (SnP_3) has been reported in the 1970's with a trigonal space group of $R\bar{3}m$ and was prepared in experiment by two stages [37]. The structure of SnP_3 can be characterized as a layered structure similar to that of arsenic in which the duplicate layers are composed of puckered honeycomb P_6 rings as shown in FIG. 1. The resulting layers are stacked perpendicular to each other along the c axis, creating a distorted octahedral environment of phosphorus atoms around each tin atom. Compared to other layered nanomaterials that have been exfoliated from their bulk crystals [38–41], the fabrication of SnP_3 layers should be a reachable goal.

By means of *ab initio* density functional calculations, we have comprehensively studied the stability, electronic, and optoelectronic properties of 2D SnP_3. The 1L SnP_3 shows a small indirect band gap of 0.71 eV, while 2L SnP_3 has a bigger band gap of 1.03 eV. Besides, 2L SnP_3 possesses a high hole (electron) mobility of about 9.171×10^4 $cm^2\cdot V^{-1}\cdot s^{-1}$ (0.3×10^4 $cm^2\cdot V^{-1}\cdot s^{-1}$). Moreover, the two-dimensional SnP_3 shows strong light harvesting ability in the visible and infrared regions, which suggests it is a promising material for ultrathin and flexible photovoltaic solar cells and optoelectronic devices.

II. METHODS

Within the framework of density functional theory (DFT), all calculations were performed with a

*Authors to whom correspondence should be addressed. E-mail: thu@njust.edu.cn, ekan@njust.edu.cn

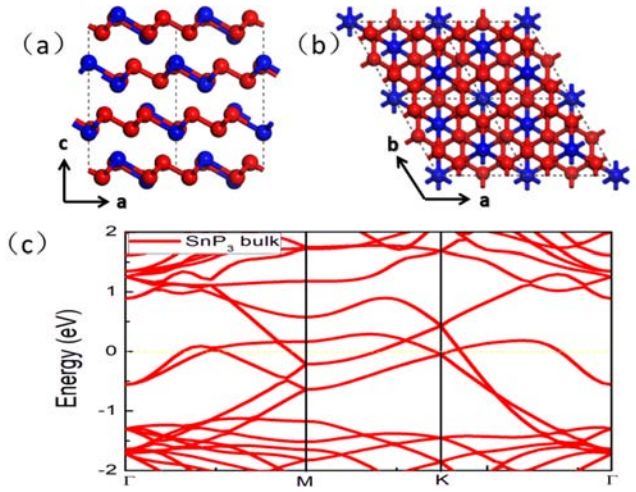

FIG. 1 Structure of bulk SnP_3 in a 2×2×1 supercell from (a) side and (b) top views. Red and blue balls represent P and Sn atoms, respectively. (c) Calculated band structure of bulk SnP_3.

projector-augmented wave method [42] as implemented in the Vienna *ab initio* simulation package (VASP) [43]. The generalized gradient approximation with Perdew-Burke-Ernzerhof method (GGA-PBE) [44] was applied as the exchange-correlation functional, and the density functional dispersion correction (D3-Grimme) [45] was adopted for a better description of the van der Waals interactions between layers. A cutoff energy of 500 eV was set for the plane wave basis. The convergence criteria for electronic and ionic relaxations are 1×10^{-6} eV per atom and 1×10^{-2} eV/Å, respectively. Γ-centered k-meshes of 7×7×5 and 7×7×1 were used for bulk and 2D unit cells, respectively. To minimize the interlayer interactions under the periodic boundary condition, a vacuum of 20 Å was constructed perpendicular to the layer plane for the monolayer and bilayer SnP_3. The phonon calculations were performed using a 4×4×1 supercell with the finite displacement method [46–48]. The cleavage energy ($E_{\rm cl}$) of SnP_3 thin layer is defined as: $E_{\rm cl}=E_{n\rm L}+E_{\rm bulk-}{}_{n\rm L}-E_{\rm bulk}$, where $E_{n\rm L}$, $E_{\rm bulk-}{}_{n\rm L}$, and $E_{\rm bulk}$ are the total energies of 1L or 2L SnP_3, the total energy of the bulk after exfoliation, and the total energy of the bulk before exfoliation, respectively. Here, a 6L SnP_3 slab is used as a model of the bulk. Larger value of $E_{\rm cl}$ indicates more difficulties to cleave SnP_3 layers from the bulk. The carrier mobility (μ) in 2D materials is calculated based on the deformation potential theory [49] and can be expressed as:

$$\mu_{\rm 2D} = \frac{2e\hbar^3 C_{\rm 2D}}{r} 2k_{\rm B}T|m^*|{E_1}^2$$
$$C_{\rm 2D} = (\partial^2 E/\partial\varepsilon^2)/S_0$$

where $C_{\rm 2D}$ is the elastic modulus, ε is the applied uniaxial strain, and S_0 is the area of the optimized supercell. m^* is the effective mass of electron and hole along the armchair and zigzag directions, which can be calculated from the derivatives of electronic bands according to $m^*=\hbar^2[\partial^2E(k)/\partial k^2]^{-1}$. E_1 is the deformation-potential constant, defined as $\Delta E=E_1(l/l_0)$, where ΔE is the shift of the band edge positions with respect to the lattice dilation l/l_0 along the zigzag and armchair directions of the orthogonal cell. The absorption coefficients were derived from the dielectric functions [53]: $\alpha(\omega)=\sqrt{2}\omega[\sqrt{{\varepsilon_1}^2(\omega)+{\varepsilon_2}^2(\omega)}-\varepsilon_1(\omega)]^{1/2}$. The imaginary part of the dielectric functions $\varepsilon_2(\omega)$ was obtained by summation over empty states, while the real part $\varepsilon_1(\omega)$ was calculated according to the usual Kramers-Kronig transformation [50–52]. Finally, all components of the absorption spectra and related optical quantities could be determined.

III. RESULTS AND DISCUSSION

Bulk tin triphosphide possesses van der Waals layers stacking along the c direction, as shown in FIG. 1 (a) and (b). The identical layers consist of puckered P_6 rings connected by Sn atoms. The centers of the P_6 rings are situated between Sn atoms of adjacent layers. In each layer of SnP_3, each Sn atom forms three Sn−P bonds with three neighboring P atoms, and each P atom forms two P−P bonds and one Sn−P bond with neighboring P and Sn atoms, respectively. The optimized lattice constants of bulk SnP_3 are a=b=7.41 Å and c=10.43 Å, which are in good agreement with the experimental results (a=b=7.38 Å and c=10.51 Å) [37]. The bond lengths and bond angles for bulk SnP_3 are summarized in Table S1 (see supplementary materials) and compared with those obtained from experimental studies. The calculated electronic structure of the bulk SnP_3 crystal is shown in FIG. 1(c), which is metallic with bands spreading across the Fermi level.

Micromechanical cleavage and liquid exfoliation are standard techniques to fabricate single layers from layered bulk materials if the cleavage energy is low. To examine the feasibility of isolation of the SnP_3 monolayer and bilayer sheets, we have calculated the cleavage energy by introducing a fracture in the bulk SnP_3. Here, a 6L SnP_3 slab is used as a model of the bulk. The cleavage energy under variation of the separation d between the fractured parts is computed to simulate the exfoliation process and the results are plotted in FIG. 2. It can be seen that the energy increases with the separation d and gradually converges to the ideal cleavage cohesion energy of about 1.06 and 0.62 J/m^2 for monolayer and bilayer SnP_3, respectively. When layers are separated from the bulk, the cleavage energy is required as the energy difference of separated layers and the bulk. Compared to monolayer SnP_3, bilayer SnP_3 is more stable than the separated two monolayer. Namely, the cleavage energy is smaller for bilayer. Compared with that of graphene (0.37 J/m^2) [53], the calculated exfoliation energy of SnP_3 is higher on the same

DOI:10.1063/1674-0068/cjcp1809212

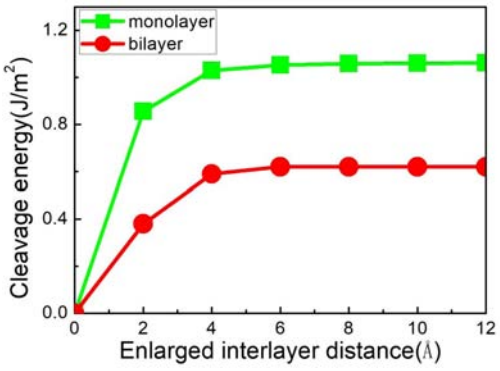

FIG. 2 Cleavage energy estimation for the formation of 1L and 2L SnP_3, calculated by enlarging the interlayer distance between the 1L/2L system that is removed from the remainder of a 6L slab, resembling the bulk model.

order of magnitude, indicating that both monolayer and bilayer of SnP_3 could be prepared experimentally using similar approaches of graphene by mechanical cleavage or liquid phase exfoliation.

The optimized structures of monolayer and bilayer SnP_3 are shown in FIG. 3. The structural characteristics of the 2D SnP_3 still remain with a hexagonal honeycomb in the same layer, but exhibit a lattice shrinkage which leads to more obvious puckering than the bulk, as shown in FIG. 3 (a) and (c). The optimized lattice parameters of 1L SnP_3 is a=b=7.15 Å and the lattice shrinkage is 3.5%, which is attributed to the change of bond length and bond angle from bulk to monolayer, as illustrated in Table S1 (see supplementary materials). The optimized lattice parameters of 2L SnP_3 is a=b=7.23 Å, being slightly larger than that of monolayer, and the structure details also can be seen in Table S1 (see supplementary materials).

In order to investigate the stabilities of monolayer and bilayer SnP_3, we have calculated their phonon dispersion curves and no imaginary phonon modes are observed, as shown in FIG. 3 (b) and (d), which confirms the dynamic stability of 2D SnP_3. The highest frequency mode of 1L SnP_3 reaches 524 cm^{-1}, which is slightly higher than that of GeP_3 (480 cm^{-1}) and comparable to silicene (580 cm^{-1}) [33, 54], indicating the mechanical robustness of the covalent P−P bonds.

Having established the stability of 2D SnP_3, we now turn our attention to their electronic properties. The band structures of monolayer and bilayer SnP_3 are calculated by using DFT-PBE method, and both structures are semiconductors as shown in FIG. 4. The monolayer SnP_3 has an indirect band gap of about 0.43 eV. The conductor band minimum (CBM) locates at the Γ point, while the valence band maximum (VBM) is between the M and K points, which is just slightly higher in energy than the K point. The calculated band structure of 2L SnP_3 (FIG. 4(b)) illustrates that 2L SnP_3 is a semiconductor with an indirect band gap of 0.61 eV. Similar to 1L SnP_3, CBM and VBM of 2L SnP_3 locate at the Γ point and M-K point, respectively. Both VBM and CBM are mostly contributed by the 3p orbitals of P and and 5p orbitals of Sn atoms, as shown in FIG. 4 (c) and (d). It is well known that GGA-PBE within DFT framework would underestimate band gap in materials. Therefore we also used the HSE06 functional to study their energy gaps. The revised energy-gap values are 0.71 eV and 1.03 eV for 1L and 2L SnP_3, respectively. Moreover, we calculate band gaps of 3L SnP_3, as shown in FIG. S1(a) (see supplementary materials), which shows metallic behavior. Obviously, with the increase in the numbers of layers from 1L to 3L, there is an abnormality in the band gap change of 2D SnP_3. From FIG. 4 (a) and (b), we can see the VBM of 2L SnP_3 is lowered and the CBM is raised, due to the intra-layer coupling. The anti-bonding orbit of P and Sn coupling increases energy of the CBM and the band gap of bilayer SnP_3. Calculated electronic density of states of P orbits for monolayer and bilayer are shown in FIG. S1 (b) and (c) (see supplementary materials), respectively.

We also studied the effects of electric field on the band structure of 1L and 2L SnP_3. As shown in FIG. 5 (a) and (b), the band gaps decrease under electric field. The band gap of 1L SnP_3 is decreased to 0.17 eV when the electric field is 0.5 eV/Å and 2L SnP_3 turns to be metallic when the electric field is 0.02 eV/Å. From FIG. S2(a) (see supplementary materials), the CBM of 1L SnP_3 is contributed by p orbit of Sn and p orbit of P, the charge density in FIG. S2 (b) and (c) (see supplementary materials) indicates the anti-bonding orbit between Sn and P reduces the band energy, resulting in the smaller gap. Therefore, the electronic properties can be turned effectively by electric field, which could lead to wide applications in electronics.

An understanding of the electronic conductance of the 1L and 2L SnP_3 can be gained from the carrier mobility calculations based on the deformation potential (DP) theory [49], the calculated deformation potential constant, in-plane stiffness, effective mass, and carrier mobility are provided in Table I and FIG. S3 (see supplementary materials). The carrier mobility for holes of 2L SnP_3 is much higher than that of 1L SnP_3, which is expected from the band structure (smaller effective mass and bigger in-plane stiffness). The 2L SnP_3 possesses a high carrier mobility of 9.171×10^4 $cm^2\cdot V^{-1}\cdot s^{-1}$ for holes along the armchair direction and 5.565×10^4 $cm^2\cdot V^{-1}\cdot s^{-1}$ for holes along the zigzag direction, which are comparable to those of phosphorene ($\sim10^4$ $cm^2\cdot V^{-1}\cdot s^{-1}$) [55]. The excellent performance of hole mobility provides a great chance for SnP_3 2D crystal to be used as the hole transport material for other materials.

The predicted SnP_3 monolayer (bilayer) has an indirect band gap of 0.71 eV (1.03 eV), which is close to that of silicon (1.16 eV) and is desirable for optoelectronic devices in experiments. Therefore, we have assessed the

DOI:10.1063/1674-0068/cjcp1809212

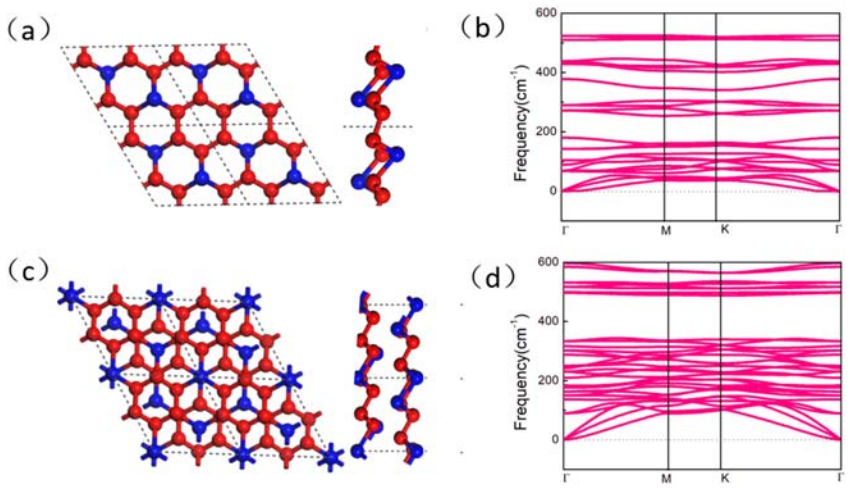

FIG. 3 (a) Structure (top and side views) and (b) phonon spectrum of 1L SnP_3, (c) structure and (d) phonon spectrum of 2L SnP_3.

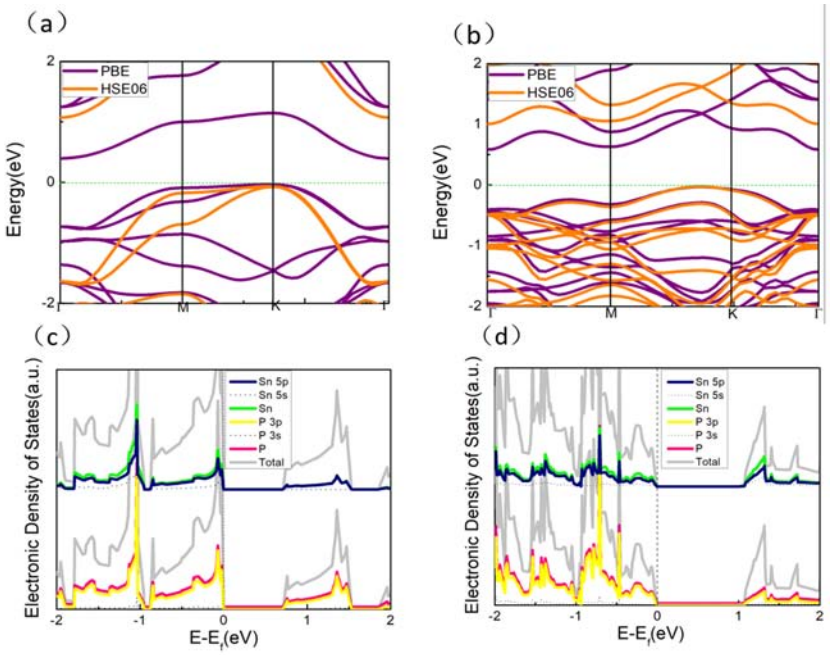

FIG. 4 Band structures of (a) 1L SnP_3 and (b) 2L SnP_3 calculated at PBE and HSE06 levels of theory. Electronic density of states of (c) monolayer and (d) bilayer.

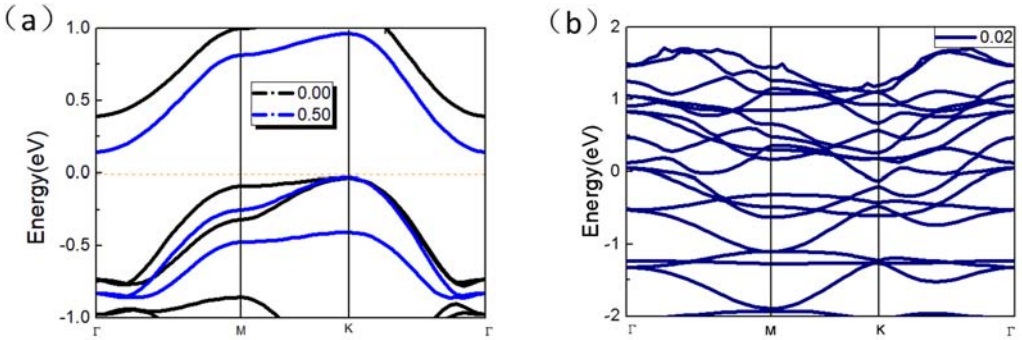

FIG. 5 Band structures of (a) 1L SnP_3 calculated under electric field (0.5 eV/Å) and (b) 2L SnP_3 calculated under electric field (0.02 eV/Å).

DOI:10.1063/1674-0068/cjcp1809212

TABLE I Calculated effective mass $|m^*|$, DP constant $|E_1|$, in-plane stiffness C_{2D}, carrier mobility μ for SnP_3 monolayer and bilayer along the zigzag (x) direction and armchair (y) directions. N_L represents the layer number of SnP_3.

Carrier type	N_L	$\lvert m^*_{zig}\rvert/m_0$	$\lvert m^*_{arm}\rvert/m_0$	$\lvert E_1\rvert$/eV		C_{2D}/(N/m)		$\mu/(10^3\ cm^2{\cdot}V^{-1}{\cdot}s^{-1})$	
				$\lvert E_{1zig}\rvert$	$\lvert E_{1arm}\rvert$	C_{zig}	C_{arm}	μ_{zig}	μ_{arm}
Electron	1	1.51	1.05	2.43	2.56	25.65	25.79	0.03	0.05
	2	0.17	0.29	2.09	2.08	60.14	77.83	6.67	3.00
Hole	1	2.87	0.74	0.77	0.92	25.65	25.79	0.07	0.80
	2	1.23	1.09	0.10	0.10	60.14	77.83	55.65	91.71

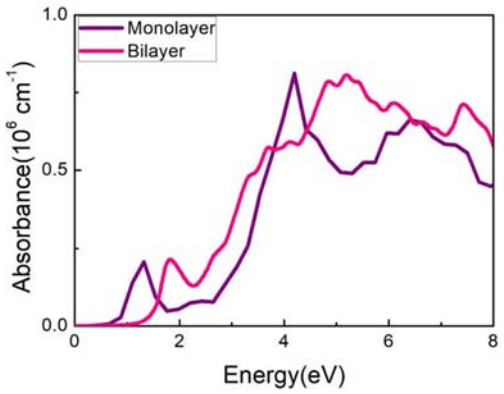

FIG. 6 Calculated in-plane (x-y) absorption spectra for 1L and 2L SnP_3 2D structures at the PBE level.

optical performance by calculating the absorption coefficients of 1L and 2L SnP_3. As shown in FIG. 6, 1L and 2L SnP_3 exhibit excellent light harvesting ability in the important region from 1 eV to 4 eV, which covers the entire visible solar spectrum. And the in-plane absorption coefficients reach the order of 106 cm^{-1} which are comparable to those of organic perovskite solar cells [56]. This remarkable optical performance indicates that 2D SnP_3 is a very promising material for efficient photovoltaic solar cells and optoelectronic devices.

IV. CONCLUSION

In summary, we have predict two-dimensional SnP_3 as a new semiconducting material with remarkable properties for nanoelectronic and optoelectronic applications. Monolayer and bilayer 2D SnP_3 are calculated to be semiconductors with indirect band gaps of 0.71 and 1.03 eV, respectively. The calculated cleavage energies of SnP_3 monolayer (1.06 J/m^2) and bilayer (0.62 J/m^2) indicate the possibility of exfoliation from the bulk. Moreover, SnP_3 bilayer has a quite high carrier mobility for holes, which is about 9.171×10^4 $cm^2{\cdot}V^{-1}{\cdot}s^{-1}$ along the armchair direction and 5.565×10^4 $cm^2{\cdot}V^{-1}{\cdot}s^{-1}$ along the zigzag direction. In addition, 2D SnP_3 shows a high optical absorbance of 106 cm^{-1} in the entire visible solar spectrum. All these excellent features make 2D SnP_3 a prospective candidate for nanoelectronics.

Supplementary materials: The atomic positions and lattice parameters are included. Besides, the band structure of 3L SnP_3, the electronic structures and charge density of 1L and 2L SnP_3, and the method of calculating the mobility are also included.

V. ACKNOWLEDGMENTS

This work was supported by the National Natural Science Foundation of China (No.11604146, No.51522206, and No.11774173), a Project Funded by the Priority Academic Program Development of Jiangsu Higher Education Institutions, Outstanding Youth Fund of Nanjing Forestry University (NLJQ2015-03), and the Fundamental Research Funds for the Central Universities (No.30915011203). We also acknowledge the support from the Shanghai Supercomputer Centre.

[1] K. S. Novoselov, A. K. Geim, S. Morozov, D. Jiang, Y. Zhang, S. Dubonos, I. Grigorieva, and A. Firsov, Science **306**, 666 (2004).
[2] K. Novoselov, A. K. Geim, S. Morozov, D. Jiang, M. Katsnelson, I. Grigorieva, S. Dubonos, and A. Firsov, Nature **438**, 197 (2005).
[3] A. K. Geim and K. S. Novoselov, Nat. Mater **6**, 183 (2007).
[4] M. J. Allen, V. C. Tung, and R. B. Kaner, Chem. Rev. **110**, 132 (2010).
[5] C. N. R. Rao, A. K. Sood, K. S. Subrahmanyam, and A. Govindaraj, Angew. Chem. Int. Ed. **48**, 7752 (2009).
[6] J. N. Coleman, M. Lotya, A. O'Neill, S. D. Bergin, P. J. King, U. Khan, K. Young, A. Gaucher, S. De, R. J. Smith, I. V. Shvets, S. K. Arora, G. Stanton, H. Y. Kim, K. Lee, G. T. Kim, G. S. Duesberg, T. Hallam, J. J. Boland, J. J. Wang, J. F. Donegan, Jaime C. Grunlan, G. Moriarty, A. Shmeliov, R. J. Nicholls, J. M. Perkins, E. M. Grieveson, K. Theuwissen, D. W. McComb, P. D. Nellist, and V. Nicolosi, Science **331**, 568 (2011).
[7] H. Okamoto, Y. Kumai, Y. Sugiyama, T. Mitsuoka, K. Nakanishi, T. Ohta, H. Nozaki, S. Yamaguchi, S. Shirai, and H. Nakano, J. Am. Chem. Soc. **132**, 2710 (2010).
[8] G. Du, Z. Guo, S. Wang, R. Zeng, Z. Chen, and H. Liu, Chem. Commun. **46**, 1106 (2010).

DOI:10.1063/1674-0068/cjcp1809212

[9] K. Chang and W. Chen, Chem. Commun. **47**, 4252 (2011).
[10] Z. Zhang, X. Liu, B. I. Yakobson, and W. Guo, J. Am. Chem. Soc. **134**, 19326 (2012).
[11] K. J. Koski and Y. Cui, ACS Nano **7**, 3739 (2013).
[12] X. Li, X. Wu, and J. Yang, J. Am. Chem. Soc. **136**, 11065 (2014).
[13] L. M. Yang, V. Bacic, I. A. Popov, A. I. Boldyrev, T. Heine, T. Frauenheim, and E. Ganz, J. Am. Chem. Soc. **137**, 2757 (2015).
[14] H. Zhang, Y. Li, J. Hou, K. Tu, and Z. Chen, J. Am. Chem. Soc. **138**, 5644 (2016).
[15] J. Theerthagiria, R. A. Senthila, B. Senthilkumarb, A. R. Poluc, J. Madhavana, and M. Ashokkumard, J. Solid State Chem. **252**, 43 (2017).
[16] N. Miao, B. Xu, N. C. Bristowe, J. Zhou, and Z. M. Sun, J. Am. Chem. Soc. **139**, 11125 (2017).
[17] K. F. Mak, C. Lee, J. Hone, J. Shan, and T. F. Heinz, Phys. Rev. Lett. **105**, 136805 (2010).
[18] A. Splendiani, L. Sun, Y. B. Zhang, T. S. Li, J. Kim, C. Y. Chim, G. Galli, and F. Wang, Nano Lett. **10**, 1271 (2010).
[19] R. Ganatra and Q. Zhang, ACS Nano **8**, 4074 (2014).
[20] K. F. Mak and J. Shan, Nat. Photonics **10**, 216 (2016).
[21] M. Stephen, A. Rafik, B. Creighton, M. W. Robert, and L. H. Christopher, ACS Nano **8**, 2880 (2014).
[22] Y. Chen, S. X. Huang, X. Ji, K. Adepalli, K. Yin, X. Ling, X. W. Wang, J. M. Xue, M. Dresselhaus, J. Kong, and B. Yildiz, ACS Nano **12**, 2569 (2018).
[23] L. Li, Y. Yu, G. J. Ye, Q. Ge, X. Ou, H. Wu, D. Feng, X. H. Chen, and Y. Zhang, Nat. Nanotechnol. **9**, 372 (2014).
[24] Z. Zhuo, X. Wu, and J. Yang, J. Am. Chem. Soc. **138**, 7091 (2016).
[25] S. Zhang, J. Yang, R. J. Xu, F. Wang, W. F. Li, M. Ghufran, Y. W. Zhang, Z. F. Yu, G. Zhang, Q. H. Qin, and Y. R. Lu, ACS Nano **8**, 9590 (2014).
[26] J. Yang, R. J. Xu, J. J. Pei, Y. W. Myint, F. Wang, Z. Wang, S. Zhang, Z. F. Yu, and Y. R. Lu, Light Sci. Appl. **4**, e312 (2015).
[27] A. Castellanos-Gomez, L. Vicarelli, E. P, Joshua. O. Island, K. L. Narasimha-Acharya, S. I. Blanter, D. J. Groenendijk, M. Buscema, G. A. Steele, and J. V. Alvarez, 2D Mater **1**, 025001 (2014).
[28] J. O. Island, G. A. Steele, H. S. van der Zant, and A. Castellanos-Gomez, 2D Mater **2**, 011002 (2015).
[29] C. Y. Zhi, Y. Bando, C. C. Tang, H. Kuwahara, and D. Golberg, Adv. Mater **21**, 2889 (2009).
[30] R. J. Chang, X. C. Wang, S. S. Wang, Y. W. Sheng, B. Porter, and H. Bhaskaran, Chem. Mater. **29**, 6252 (2017).
[31] L. Song, L. J. Ci, H. Lu, P. B. Sorokin, C. H. Jin, J. Ni, A. G. Kvashnin, D. G. Kvashnin, J. Lou, B. I. Yakobson, and P. M. Ajayan, Nano. Lett. **10**, 3209 (2010).
[32] S. Zhang, Z. Yan, Y. Li, Z. Chen, and H. Zeng, Angew. Chem. Int. Ed. **54**, 3112 (2015).
[33] Y. Jing, Y. D. Ma, Y. F. Li, and T. Heine, Nano Lett. **17**, 1833 (2017).
[34] Y. D. Ma, A. Kuc, and T. Heine, J. Am. Soc. **139**, 11694 (2017).
[35] Y. D. Ma, A. Kuc, Y. Jing, P. Philipsen, and T. Heine, Angew. Chem. Int. Ed. **56**, 10214 (2017).
[36] N. Lu, Z. W. Zhuo, H. Y. Guo, P. Wu, W. Fa, and X. J. Wu, J. Phys. Chem. Lett. **9**, 1728 (2018).
[37] J. Gullman and O. Olofsson, J. Solid State Chem. **5**, 441 (1972).
[38] R. Zacharia, H. Ulbricht, and T. Hertel, Phys. Rev. B: Condens. Matter Mater. Phys. **69**, 155406 (2004).
[39] S. Zhao, Z. Li, and J. Yang, J. Am. Chem. Soc. **136**, 13313 (2014).
[40] Y. Jiao, F. Ma, G. Gao, J. Bell, T. Frauenheim, and A. Du, J. Phys. Chem. Lett. **6**, 2682 (2015).
[41] F. Li, X. Liu, Y. Wang, and Y. Li, J. Mater. Chem. C **4**, 2155 (2016).
[42] P. E. Blochl, Phys. Rev. B: Condens. Matter Mater. Phys. **50**, 17953 (1994).
[43] J. Hafner, J. Comput. Chem. **29**, 2044 (2008).
[44] J. P. Perdew, K. Burke, and M. Ernzerhof, Phys. Rev. Lett. **77**, 3865 (1996).
[45] S. Grimme, J. Antony, S. Ehrlich, and H. Krieg, J. Chem. Phys. **132**, 154104 (2010).
[46] G. Kresse, J. Furthmüller, and J. Hafner, EPL **32**, 729 (1995).
[47] K. Parlinski, Z. Q. Li, and Y. Kawazoe, Phys. Rev. Lett. **78**, 4063 (1997).
[48] A. Togo and I. Tanaka, Scr. Mater. **108**, 1 (2015).
[49] J. Bardeen and W. Shockley, Phys. Rev. **80**, 72 (1950).
[50] S. Saha, T. Sinha, and A. Mookerjee, Phys. Rev. B: Condens. Matter Mater. Phys. **62**, 8828 (2000).
[51] R. King-Smith and D. Vanderbilt, Phys. Rev. B: Condens. Matter Mater. Phys. **47**, 1651 (1993).
[52] M. Gajdoš, K. Hummer, G. Kresse, J. Furthmüller, and F. Bechstedt, Phys. Rev. B: Condens. Matter Mater. Phys. **73**, 045112 (2006).
[53] R. Zacharia, H. Ulbricht, and T. Hertel, Phys. Rev. B: Condens. Matter Mater. Phys. **69**, 155406 (2004).
[54] S. Cahangirov, M. Topsakal, E. Aktürk, H. Sahin, and S. Ciraci, Phys. Rev. Lett. **102**, 236804 (2009).
[55] J. Qiao, X. Kong, Z. X. Hu, F. Yang, and W. Ji, Nat. Commun. **5**, 4475 (2014).
[56] M. Shirayama, H. Kadowaki, T. Miyadera, T. Sugita, M. Tamakoshi, M. Kato, T. Fujiseki, D. Murata, S. Hara, T. N. Murakami, S. Fujimoto, M. Chikamatsu, and H. Fujiwara, Phys. Rev. Appl. **5**, 014012 (2016).

DOI:10.1063/1674-0068/cjcp1809212